Chinese Chemical Letters 37 (2026) 112085

Contents lists available at ScienceDirect

Chinese Chemical Letters

journal homepage: www.elsevier.com/locate/cclet

Macro-micro spray characteristics of nasal spray: Bridging physicochemical properties to precision olfactory delivery

Xi Kong[a,b,1], Guanlin Wang[c,1], Shuhua Wei[a], Kaiqing Zhang[a], Yihong Gao[a], Xiaofan Li[a], Chuangxin Chen[a], Ziyu Zhao[a,b,*], Chuanbin Wu[a,b,*], Xuejuan Zhang[a,b,*]

[a] State Key Laboratory of Bioactive Molecules and Druggability Assessment, Guangdong Basic Research Center of Excellence for Natural Bioactive Molecules and Discovery of Innovative Drugs, Jinan University, Guangzhou 511443, China
[b] College of Pharmacy, Jinan University, Guangzhou 511443, China
[c] School of Pharmaceutical Sciences, Sun Yat-sen University, Guangzhou 510006, China

ARTICLE INFO

Article history:
Received 6 April 2025
Revised 6 November 2025
Accepted 6 November 2025
Available online 8 November 2025

Keywords:
Nose-to-brain drug delivery
Olfactory deposition
Viscosity-regulated strategy
Macroscopic spray geometry
Microscopic droplet dynamic

ABSTRACT

The nose-to-brain drug delivery system has emerged as a transformative strategy for central nervous system (CNS) diseases therapy by leveraging the olfactory pathway to circumvent the blood-brain barrier. However, its clinical translation remains impeded by suboptimal olfactory deposition efficiency. A critical but poorly understood challenge lies in rational formulation design, particularly regarding how key physicochemical properties like viscosity govern the nasal drug delivery processes. Using rizatriptan nasal sprays as a viscosity-regulated model system (2–250 mPa s), we dissected how formulation viscosity governs olfactory deposition through synchronized macro-micro spray characteristics. A module 3D-printed human nasal cast was utilized to assess the olfactory deposition efficiency. Additionally, the spray pattern, plume geometry and real-time droplet size distribution were examined using laser diffraction analysis. The results demonstrate a non-monotonic olfactory deposition dependence on viscosity, peaking at 40 mPa s with 31.64 % efficiency (31-fold enhancement *vs.* 2 mPa s). Furthermore, the increase of viscosity led to a reduction in plume angle and spray area, while simultaneously decreasing the stabilization stage fraction of droplets. Mechanistic analysis revealed two competing viscosity-mediated effects: (1) Macroscale plume narrowing that minimized anterior nasal losses; (2) Microscale destabilization of droplets that impaired turbinate transportation. This study elucidates that the viscosity-regulated precision olfactory deposition results from the equilibrium between macroscopic spray geometry and microscopic droplet dynamic, challenging the conventional single-parameter optimization paradigm. Our findings advance nose-to-brain drug delivery by deciphering the viscosity-regulated deposition mechanism, thereby paving the way for rationally designed nasal sprays with enhanced targeting efficiency for CNS diseases.

© 2026 Published by Elsevier B.V. on behalf of Chinese Chemical Society and Institute of Materia Medica, Chinese Academy of Medical Sciences.

The global aging population has driven a concerning rise in central nervous system (CNS) diseases, including Alzheimer's disease, Parkinson's disease, amyotrophic lateral sclerosis, stroke, gliomas. There are over 300 million cases of CNS diseases worldwide in 2021, establishing them as a leading cause of global health burdens [1,2]. While therapeutic development for these conditions remains a research priority, progress has been fundamentally constrained by the blood-brain barrier (BBB), which blocks over 98 % of systemically administered drugs from reaching the brain [3–5]. Current strategies to overcome the BBB face critical limitations: Intracerebroventricular injections enable direct CNS delivery but require invasive, anesthesia-dependent procedures unsuitable for chronic use [6]. Focused ultrasound-mediated BBB permeabilization risks pathogen infiltration through transient BBB openings [7]. Nanocarriers, though enhancing BBB penetration, retain systemic exposure risks and suboptimal brain targeting efficiency inherent to intravenous administration [8,9]. These challenges underscore the urgent need for non-invasive drug delivery systems capable of achieving efficient, localized brain targeting.

In response, nasal drug delivery system (NDDS) *via* olfactory pathway has emerged as a promising transformative strategy for brain drug delivery [10]. This approach circumvents the BBB, enabling direct delivery of active pharmaceutical ingredients to the

* Corresponding authors.
E-mail addresses: zhaoziyu0515@163.com (Z. Zhao), chuanbinwu@jnu.edu.cn (C. Wu), zhanghongdou0223@126.com (X. Zhang).
[1] These authors contributed equally to this work.

https://doi.org/10.1016/j.cclet.2025.112085
1001-8417/© 2026 Published by Elsevier B.V. on behalf of Chinese Chemical Society and Institute of Materia Medica, Chinese Academy of Medical Sciences.

brain [11]. Extensive research has demonstrated that intranasal administration provides significantly higher brain bioavailability and reduces systemic exposure compared to conventional dosage forms [12–14]. Despite the theoretically promising advantages of NDDS for efficient brain drug delivery, clinical studies have demonstrated that the cerebrospinal fluid-to-plasma concentration ratio of existing NDDS products remains <0.1, which is significantly lower than the design expectations [15–17]. Consequently, enhancing the nose-to-brain drug delivery efficiency of NDDS has become a critical focus in pharmaceutical research.

To address this, researchers have proposed adhesion retention strategies and absorption enhancement strategies [18–20]. While these approaches can increase brain drug exposure to some extent, the improvement in nose-to-brain drug delivery efficiency remains suboptimal. Fundamentally, these strategies emphasize the regulation of post-deposition behavior but lack intervention during the nasal delivery process. Based on the anatomical and physiological structure, the nasal cavity can be divided into the nasal vestibule (NV), respiratory region, and olfactory region, with the latter being critical for nose-to-brain drug delivery [21]. Numerous studies have documented the effects of various formulation properties (such as viscosity, surface tension, and rheological behavior) on olfactory deposition [22–24]. However, a critical but poorly understood challenge lies in rational formulation design, particularly regarding how key physicochemical properties govern the nasal delivery process. We posit that the fundamental mechanism of nasal drug delivery lies in the interaction between aerosolized sprays and the anatomical and physiological features of the nasal cavity. Consequently, spray characteristics may serve as a critical determinant in linking the formulation physicochemical properties to olfactory deposition.

In our previous study, we established that formulation viscosity serves as a critical factor influencing the nasal delivery process [25]. Our findings indicated that adjusting the formulation viscosity could enhance the olfactory deposition efficiency. Furthermore, we initially validated a correlation between olfactory deposition efficiency and brain drug exposure in a rat model ($R^2 = 0.7755$). Nevertheless, the relationship between formulation viscosity and olfactory deposition is non-monotonic, and the specific regulatory mechanism remains unclear, thereby restricting the application of these findings in the development of nose-to-brain drug delivery systems.

In this study, we systematically investigated how formulation viscosity governs olfactory deposition through synchronized macro-micro spray characteristics. Specifically, we prepared viscosity-regulated model nasal spray (2–250 mPa s) according to previously reported method [25,26], and systematically characterized the fundamental properties of all formulations. There was no significant difference in physicochemical properties except viscosity (Figs. 1A–C). Pump delivery uniformity (~100 mg/actuation) complied with Food and Drug Administration (FDA) standards (Fig. 1D). The results suggested that the model system with gradient viscosity was successfully constructed, which could be employed to explore the influence of viscosity on olfactory deposition.

To investigate nasal distribution for viscosity-regulated model system, the modular 3D-printed human nasal cast was used (Figs. 1E and F). The nasal distribution of viscosity-regulated model system showed significant viscosity dependence (Figs. 1G and H). At lower viscosities (2–15 mPa s), the drug deposition predominantly occurred in the anterior nasal cavity, while no detectable drug levels were observed in the superior turbinate (ST). Notably, 40 mPa s formulation exhibited the highest level of ST deposition. Excessive viscosity (>100 mPa s) paradoxically increased NV deposition by 33.91 % and reduced ST delivery by 95.78 %. The above results indicated that viscosity has a significant influence on the nasal deposition of model system. Next, we further investigated the olfactory deposition efficiency (ODF) of viscosity-regulated model system. Olfactory deposition efficiency (ODF) exhibited a non-monotonic relationship with viscosity, peaking at 31.64 % for the 40 mPa s formulation (31-fold increase *vs.* 2 mPa s) (Figs. 1I and J). The results indicated that viscosity plays a significant role in olfactory deposition; however, the specific mechanism of viscosity-regulated olfactory deposition remained unclear, thereby hindering the rational design of NDDS formulations.

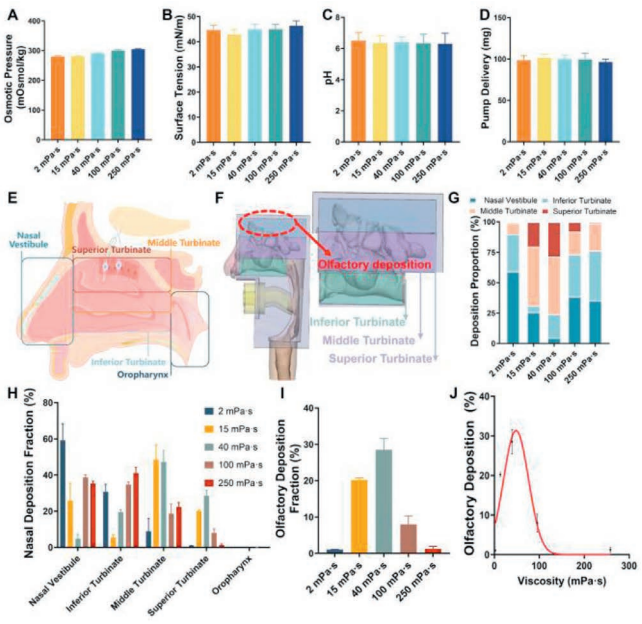


Fig. 1. Characterization of model system: (A) Surface tension, (B) osmotic pressure, (C) pH, (D) pump delivery. Nasal deposition distribution of model system: (E) Schematic diagram of human nasal, (F) schematic diagram of 3D-printed human nasal model, (G) deposition proportion, (H) nasal deposition fraction, (I) olfactory deposition fraction. (J) Correlation between viscosity and olfactory deposition. Data are presented as mean ± standard deviation (SD) ($n = 3$).

Based on the current understanding of the nasal drug delivery process, spray characteristics play a critical role in determining olfactory deposition. These characteristics can be analyzed from two perspectives: macroscopic spray geometry and microscopic droplet dynamics. However, most existing studies on spray characteristics have been conducted under unconstrained free-flow conditions, neglecting the interaction between spray characteristics and nasal anatomy. Drawing on literature reviews and findings from our prior studies, we propose that the primary limitation to olfactory deposition efficiency lies in the mismatch between spray characteristics and nasal anatomy. This mismatch is specifically reflected in the nasal valve interception and nasal turbinate sedimentation. The nasal valve interception is predominantly governed by macroscopic spray geometry, whereas nasal turbinate sedimentation is primarily determined by microscopic droplet dynamics. Consequently, considering the spatio-temporal features of the nasal anatomy, we examined the macroscopic spray characteristics at 15 mm (the distance between the nozzle and the nasal valve) and the microscopic droplet dynamics at 80 mm (the distance between the nozzle and the olfactory region) in the model system [27]. Macroscopic spray geometry evaluation revealed that higher-viscosity formulations generated more convergent plume angles (decreasing from 50.60° to 19.20°) and reduced plume widths (Figs. 2A–D). A convergent spray plume could minimize drug ineffective deposition in the NV and enhance the total amount of drug delivered to the nasal turbinate. Spray pattern analysis at the nasal valve (15 mm from nostril) revealed viscosity-dependent reductions in cross-sectional area. Viscosity-regulated formulations

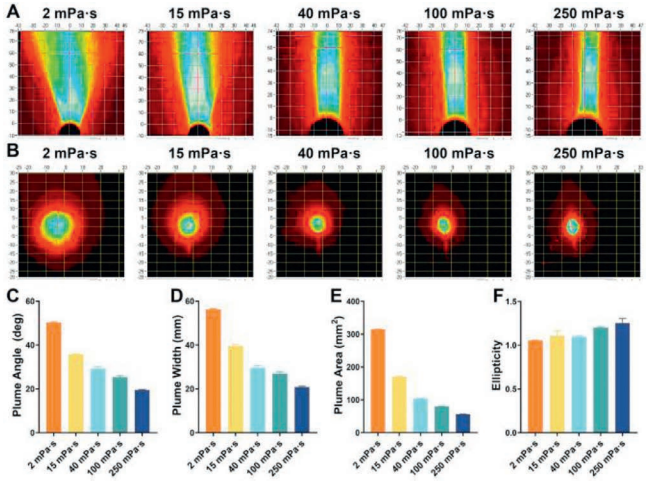


Fig. 2. Macroscopic spray geometry of model system: (A) Plume geometry images, (B) spray pattern images, (C) plume angle, (D) plume width, (E) plume area, (F) ellipticity. Data are presented as mean ± SD ($n = 3$).

(15–250 mPa s) achieved spray areas below 200 mm^2, matching the valve dimensions (Fig. 2E) [28]. While ovality ratios remained stable (~1.15) across most viscosities, 250 mPa s formulation induced irregular spray morphology and elevated ellipticity, potentially compromising deposition consistency (Fig. 2F) [29].

Despite this macroscopic analysis proved valuable for anterior nasal cavity assessment, it exhibited limited predictive capacity for posterior region deposition patterns. To assess delivery process, microscopic droplet dynamic was analyzed across clinically relevant spray distances (15–80 mm), establishing a spatial-resolved understanding of particle transport dynamics throughout the nasal cavity. The model system exhibited marginally larger droplet sizes at 15 mm compared to 30–80 mm distances (Figs. 3A–D). This size discrepancy likely stems from incomplete droplet dispersion at 15 mm, followed by dynamic fragmentation and reaggregation processes during plume development. Beyond 30 mm, droplet stabilization occurred with minimal subsequent size variations (Fig. 3B), indicating establishment of equilibrium dispersion dynamics within this critical threshold. Additionally, microscopic analysis revealed viscosity-dependent droplet dynamics. *C.opt* (optical concentration, droplet concentration indicator) exhibited a trapezoidal profile. Higher viscosity formulations demonstrated reduced $C.opt_{max}$ and $C.opt_{AUC}$, indicating impaired dispersion (Fig. 3E).

Building upon the spatial-temporal characterization of droplet dynamics, temporal analysis of the spray process revealed three distinct phases governed by coupled *C.opt* and droplet size evolution: (1) Formation stage (rapid dispersion with ascending concentration), (2) stabilization stage (particle equilibrium maintenance), and (3) dissipation stage (progressive concentration decay). Systematic quantification of these temporal regimes enabled extraction of critical kinetic parameters, total spray duration, formation stage fraction (FSF), stabilization stage fraction (SSF), and dissipation stage fraction (DSF) (Figs. 3F–I). SSF, which reflects sustained drug delivery capability, peaked at 72.62 % for the 15 mPa s formulation (Fig. 3H), indicating superior transport efficiency in the nasal turbinate. Higher viscosities prolonged formation stage duration (28.51 % increase at 250 mPa s *vs.* 2 mPa s), delaying stabilization. While spray duration (~100 ms) remained consistent across 15–250 mPa s, the stabilization stage fraction variability highlights viscosity's critical role in balancing dispersion efficiency and delivery stability. These findings underscore that moderate viscosity (15 mPa s) optimizes stabilization stage dominance, enhancing olfactory targeting potential.

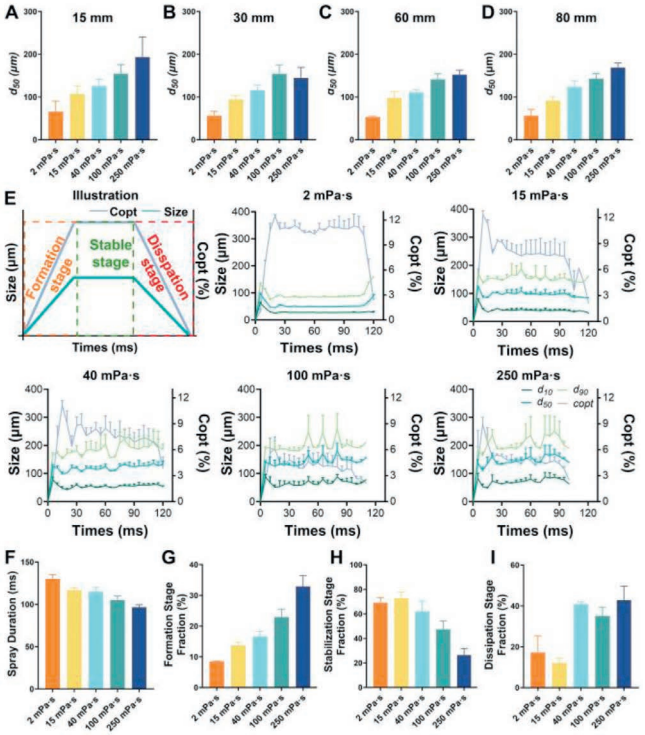


Fig. 3. The droplet size in different spray distances: (A) 15 mm, (B) 30 mm, (C) 60 mm, (D) 80 mm. The spray process of model system: (E) The time-dependent variation of droplet size, (F) spray duration, (G) formation stage fraction, (H) stabilization stage fraction, (I) dissipation stage fraction. Data are presented as mean ± SD ($n = 3$).

Based on the results of nasal deposition distribution and spray characteristics, we systematically established the correlation between physicochemical properties, spray characteristics, and olfactory deposition efficiency. Through an in-depth investigation into the interaction between macro-micro spray characteristics and nasal delivery process, we elucidated the specific mechanism of viscosity-regulated olfactory deposition. The spray characteristics of NDDS are determined by the physicochemical properties of the formulation solution and the nasal spray device. Based on the pressure swirl theory, the formulation solution generates turbulence within the nozzle and subsequently disperses to form aerosol droplets. Macroscopically, its spray geometry exhibits a near-conical divergent spray, while microscopically, it forms a dynamic aerosol droplet cloud. However, current research on spray characteristics is predominantly conducted in unconstrained free-flow fields, neglecting the interaction between the nasal delivery process and the spray characteristics. Combining the insights from previous research and our findings, we conclude that the primary cause of the low olfactory deposition efficiency is the incongruity between the spray characteristics of NDDS and the physiological structure of the nasal cavity. This is specifically evidenced by nasal valve interception and nasal turbinate sedimentation (Fig. S1 in Supporting information). Nasal valve interception: During the nasal delivery process, aerosol droplets must traverse the nasal valve to enter the respiratory region from the NV. The nasal valve represents the narrowest portion of the nasal cavity, with an average cross-sectional area of approximately 200 mm^2 in healthy adults. A paradox exists in the NV region, where the nasal structure transitions from wide to narrow, while the nasal spray disperses from narrow to wide. This phenomenon leads to significant collisional deposition of drugs within the NV, consequently reducing the olfactory deposition efficiency. Therefore, a convergent spray is necessary for nose-to-brain drug delivery. Nasal

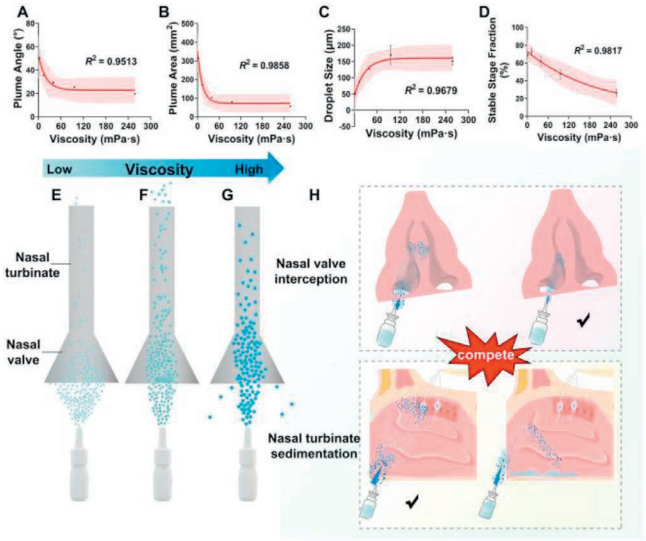


Fig. 4. The correlation between viscosity and spray characteristics: (A) Plume angle, (B) plume area, (C) droplet size, (D) stabilization stage fraction. The nasal delivery process simulation of viscosity-regulated nasal spray: (E) Low viscosity, (F) moderate viscosity and (G) excessive viscosity. (H) Schematic illustrations of viscosity-regulated olfactory deposition. Data are presented as mean ± SD ($n = 3$).

turbinate sedimentation: The olfactory region refers to the area covered by olfactory neurons, situated at the apex of the superior nasal turbinate. Consequently, the deposition of aerosol droplets in the olfactory region necessitates efficient transport capacity within the nasal turbinate. Aerosol droplets acquire initial kinetic energy during the actuation of the nasal spray device, which propels them upward against gravitational forces. As the droplets traverse the nasal turbinate, their dynamic potential energy diminishes progressively. At this stage, the aerosol droplets may begin to prematurely aggregate and settle in the nasal turbinate. In summary, the optimal olfactory deposition necessitates specific spray characteristics of NDDS. First, the spray pattern should be as convergent as possible to minimize drug retention at the nasal valve. Second, aerosol droplets must be delivered in a continuous and stable manner to prevent premature settling within the nasal turbinate.

As previously discussed, adapting spray characteristics to the nasal delivery process is crucial for achieving effective olfactory deposition. Nevertheless, the ultimate goal of NDDS development hinges on rational formulation design. Consequently, we systematically investigated the correlation between viscosity and spray characteristics, analyzed the impact of viscosity on spray characteristics, and elucidated the underlying regulatory mechanisms.

The effect of viscosity on macroscopic spray geometry: The macroscopic spray geometry is characterized by the plume angle and spray area, and the results indicate a strong correlation between viscosity and both the plume angle and spray area (Figs. 4A and B). When the formulation viscosity increased from 2 mPa s to 250 mPa s, we observed a 61.24 % reduction in plume angle from 50.23° to 19.47° ($R^2 = 0.9513$). Concurrently, the spray area decreased from 314.27 mm^2 to 55.70 mm^2 ($R^2 = 0.9858$). Based on this observation, we further investigate the regulatory mechanism of viscosity on the macroscopic spray geometry. Specifically, the macroscopic spray geometry essentially represents the trajectory of aerosol droplets during the spray process, which adheres to the Navier-Stokes momentum governing equation (Eq. 1) [30]:

$$\frac{du_d}{d_t} = F_D(u - u_d) + g(\rho_d - \rho) + F_x \quad (1)$$

where u_d, and ρ_d were the droplets velocity and droplets density, u and ρ were the fluid velocity and fluid density, g was the gravity coefficient, F_D was the drag force on the droplets, and F_x was the force other than drag force and gravity. It is worth noting that the plume angle and spray area depend on the radial force perpendicular to the spray axis, which is mainly affected by F_D:

$$F_D = \frac{18\mu C_D R_e}{24\rho_d d^2} \quad (2)$$

where μ was the hydrodynamic viscosity of spray, C_D was the drag coefficient, R_e was the relative Reynolds number, ρ_d was the droplet density and d was the droplet size. According to the Eq. 2, F_D was inversely proportional to d_d. In this study, d_d increased with the increase of formulation viscosity (Figs. 3A–D), leading to insufficient radial force on the droplets. Correspondingly, the plume angle and spray area decreased with the increase of formulation viscosity, which is conducive to olfactory deposition.

The effect of viscosity on microscopic droplet dynamic: The microscopic droplet dynamic is characterized by the droplets size and stabilization stage fraction, and the results indicate a strong correlation between viscosity and both the droplets size and stabilization stage fraction (Figs. 4C and D). When the formulation viscosity increased from 2 mPa s to 250 mPa s, the droplet size increased from 56.63 μm to 245.01 μm ($R^2 = 0.9679$). Concurrently, the stabilization stage fraction decreased from 72.62 % to 24.37 % ($R^2 = 0.9817$). Droplet size and stabilization stage fraction reflect the spatiotemporal variation of droplet size during the nasal delivery process y, which plays a crucial role in the delivery of aerosol droplets within nasal turbinate. According to the Taylor Analogy Breakup (TAB) model, as shown in Fig. S2 (Supporting information), the aerosol droplets undergo continuous fragmentation and reaggregation during the nasal delivery process (Fig. S2A), with the spatiotemporal variation of aerosol droplets being modulated by aerodynamic force (F_a), surface tension (F_σ) and viscous force (F_μ).

$$\frac{d^2y}{dt^2} = F_a - (F_\sigma + F_\mu) \quad (3)$$

$$F_a = \frac{C_F}{C_b}\frac{\rho}{\rho_d}\frac{|u - u_d|^2}{r^2} \quad (4)$$

$$F_\sigma = \frac{C_k \sigma x}{C_b \rho_d r^4} \quad (5)$$

$$F_\mu = \frac{C_d \mu_d}{\rho_d r^2}\frac{dy}{dt} \quad (6)$$

where y was the droplet deformation rate, a dimensionless parameter. ρ and u were gas density and spray velocity, ρ_d and u_d were droplet density and droplet velocity, r was droplet initial radius, σ was surface tension, and μ was viscosity. C_F, C_k, C_b and C_d were model constants.

Therefore, the spatiotemporal variation of aerosol droplets actually depends on the dynamic competition between aerodynamic force (which disrupt the droplet structure) and the combined effects of surface tension and viscous force (which preserve the droplet structure) (Fig. S2B). During the spray formation stage, the droplets possess a high initial velocity. Based on Eqs. 4–6, the aerodynamic force acting on the droplets significantly exceeds their intrinsic viscous force and surface tension, leading to droplet breakup and fragmentation (Fig. S2C). As the spray velocity attenuates, the combined force of surface tension and viscous force reaches equilibrium with the aerodynamic force. At this point, the spray transitions into a stable stage, during which the droplet size remains largely constant (Fig. S2D). However, as the spray velocity further decreases, the combined force of surface tension and viscous force becomes sufficient to counteract the

aerodynamic force. Consequently, droplets tend to collide and coalesce, forming larger droplets that settle under gravitational effect (Fig. S2E). Throughout this process, an increase in formulation viscosity enhances the droplets' viscous force, enabling them to maintain a larger droplet size. Nevertheless, when viscosity becomes excessively high, aerosol droplets enter the dissipation stage more rapidly, resulting in premature settling in the nasal turbinate, which hinders effective deposition in the olfactory region.

To summarize, our multi-faceted analysis integrating experimental data, theoretical modeling, and computational simulation reveals that viscosity regulates olfactory deposition through two competing pathways that constitute a critical trade-off. This competitive mechanism explains the observed non-monotonic relationship: while increasing viscosity improves macroscopic spray targeting, it simultaneously undermines microscopic droplet stability. Increasing the viscosity could reduce the plume angle and spray area, which is beneficial to reduce the collision deposition in the NV. However, excessive viscosity would lead to the increase of aerosol droplet variation, which further reduced the transportation distance of aerosol droplets in nasal turbinate. Correspondingly, it occurred that the aerosol droplets deposited in the nasal turbinate early, and the olfactory deposition efficiency was greatly reduced. Therefore, the influence of viscosity on both macroscopic spray geometry and microscopic droplet dynamic must be thoroughly evaluated during the development of nose-to-brain drug delivery systems.

Accordingly, we further proposed the specific mechanism of viscosity-regulated olfactory deposition. From the perspective of macroscopic spray geometry, as the formulation viscosity increased from 5 mPa s to 40 mPa s, the plume angle decreased from 50.23° to 29.33°. This resulted in a 92.07 % reduction in NV collision deposition and a 27.17-fold increase in olfactory deposition efficiency. However, when the plume angle was further reduced beyond this range, the expected trend of reduced or maintained collision deposition in the NV was not observed. Instead, the collision deposition in the NV increased by 8.17 times, while the olfactory deposition efficiency decreased by 95.78 %. This indicates that not all drug depositions in the NV are necessarily attributed to collision depositions. Microscopic droplet dynamics results revealed that when viscosity increased further from 40 mPa s to 250 mPa s, the stabilization stage fraction of aerosol droplets decreased by 57.59 %, thereby reducing the transport capacity of aerosol droplets within the nasal turbinate. Consequently, the olfactory deposition efficiency decreased from 28.53 % to 1.21 %.

The aforementioned results indicate that, within the viscosity-regulated model system, the macroscopic spray geometry and microscopic droplet dynamics exhibit antagonistic effects on the olfactory deposition efficiency. To further investigate this intricate mechanism, a simplified two-region model was developed based on the hydrodynamic characteristics of nasal delivery process (Video S1 in Supporting information). The anatomical structure of the nasal cavity is simplified as follows: (1) NV (a hollow frustum of a cone structure simulating the nasal valve interception effect); (2) nasal meatus (a hollow cylindrical structure simulating the gravitational settling effect). Additionally, boundary conditions were established wherein the collision of aerosol droplets with the nasal wall triggers *in-situ* deposition. The model simulation elucidates a three-stage mechanism of viscosity-regulated olfactory deposition: When the formulation viscosity is low ($<$15 mPa s), the nasal spray exhibits emanative plume angle and spray area, leading to a significant proportion of droplets being trapped by the nasal valve. Only a small fraction of droplets at the spray center can pass through the nasal valve and enter the nasal meatus. The simplified two-region model simulation (Figs. 4E–G) visually validates this viscosity-mediated competition and its spatial dynamics. It demonstrates that the optimal viscosity ($\sim$40 mPa s) represents a compromise where macroscopic convergence maximizes nasal valve passage while microscopic stability is still sufficient for turbinate transport. Simulations at viscosities outside this range (Figs. 4E and G) vividly depict the failure modes: excessive divergence causes valve interception at low viscosity, while excessive droplet size causes premature sedimentation at high viscosity. This simulation provides a predictive tool for visualizing the deposition outcomes of different formulation properties. This study demonstrates that the non-monotonic influence of viscosity on olfactory deposition efficiency fundamentally represents a dynamic equilibrium between macroscopic spray geometry and microscopic droplet dynamics. The optimal olfactory deposition occurs within the co-optimization range of these two factors. In brief, mechanistic analysis revealed two competing viscosity-mediated effects (Fig. 4H): (1) Macroscale plume narrowing that minimized anterior nasal losses through geometric optimization; (2) microscale droplet destabilization through size-dependent sedimentation that impaired turbinate transportation efficiency. This dual mechanism underscores the necessity of balancing macro-micro properties when engineering nasal sprays for targeted olfactory delivery.

The nose-to-brain drug delivery system is capable of bypassing the BBB and delivering drugs directly to the brain, offering a significant advantage in the treatment of CNS diseases. However, due to insufficient understanding of the nasal delivery process and regulatory mechanisms, the formulation development for nose-to-brain drug delivery systems remains largely empirical, hindering the clinical translation of these formulations. In this study, we employed a viscosity-regulated rizatriptan nasal spray as a model system to systematically investigate the correlations among physicochemical properties, spray characteristics, and olfactory deposition efficiency. Furthermore, we elucidated the two-scale mechanism underlying viscosity-regulated olfactory deposition: (1) Macroscopic spray convergence, which minimizes loss in the anterior nasal cavity; (2) microscopic instability of aerosol droplets, influencing transport depth within the nasal turbinates. Effective drug deposition in the olfactory region is fundamentally the result of a dynamic balance between macroscopic spray geometry and microscopic droplet dynamic. Our findings not only provide critical theoretical support but also establish a mechanism-driven design paradigm. The identified competition necessitates a balanced optimization approach rather than maximizing a single parameter. For rational nasal spray design, formulators must now aim for the co-optimization window where spray convergence and droplet stability are balanced, as predicted by our models and simulations. This shifts the development strategy from empirical testing to a principled, model-informed process.

Declaration of competing interest

The authors declare that they have no known competing financial interests or personal relationships that could have appeared to influence the work reported in this paper.

Acknowledgments

This study was supported by Natural Science Foundation of Guangdong Province, China (Nos. 2024A1515010896, 2025A1515010639), Science and Technology Projects in Guangzhou (No. 202102070001), Youth S&T Talent Support Programme of Guangdong Provincial Association for Science and Technology (No. SKXRC2025338).

Supplementary materials

Supplementary material associated with this article can be found, in the online version, at doi:10.1016/j.cclet.2025.112085.

References

[1] J.D. Steinmetz, K.M. Seeher, N. Schiess, et al., Lancet Neurol. 23 (2024) 344–381.
[2] G. Li, Z. Li, Y. Sun, et al., Chin. Chem. Lett. 37 (2026) 111524.
[3] S. Sau, H.O. Alsaab, S.K. Kashaw, et al., Drug Discov. Today 22 (2017) 1547–1556.
[4] S. Ruan, Y. Zhou, X. Jiang, H. Gao, Adv. Sci. 8 (2021) 2004025.
[5] D. Wu, Q. Chen, X. Chen, et al., STTT 8 (2023) 217.
[6] M. Agrawal, S. Saraf, S. Saraf, et al., Expert Opin. Drug Del. 15 (2018) 589–617.
[7] J. Park, Y. Zhang, N. Vykhodtseva, et al., J. Control. Release 162 (2012) 134–142.
[8] T. Lei, Z. Yang, C. Jiang, et al., ACS Nano 18 (2024) 3234–3250.
[9] H. Chen, M. Zhou, Y. Zeng, et al., Adv. Sci. 9 (2022) 2105854.
[10] M.D. Sweeney, Z. Zhao, A. Montagne, et al., Physiol. Rev. 99 (2019) 21–78.
[11] Y. Liu, Y. Tan, G. Cheng, et al., Adv. Mater. 36 (2024) e2307081.
[12] Y. Long, Q. Yang, Y. Xiang, et al., Pharmacol. Res. 159 (2020) 104795.
[13] X. Yang, W. Yang, X. Xia, et al., Small 18 (2022) e2203182.
[14] M. Agrawal, S. Saraf, S. Saraf, et al., J. Control. Release 281 (2018) 139–177.
[15] P. Henriques, A. Fortuna, S. Doktorovová, Eur. J. Pharm. Biopharm. 176 (2022) 1–20.
[16] M.R. Bouw, S.S. Chung, B. Gidal, et al., Epilepsy Res. 171 (2021) 106567.
[17] T. Liu, B.Q. Lu, D.D. Wang, et al., Evid. Based. Complement. Alternat. Med. 2022 (2022) 4666332.
[18] C.P. Costa, J.N. Moreira, J.M. Sousa Lobo, A.C. Silva, Acta Pharm. Sin. B 11 (2021) 925–940.
[19] N. Shrestha, S. Khan, Y.R. Neupane, et al., Polymers 12 (2020) 2589.
[20] M. Perkušić, L. Nižić Nodilo, I. Ugrina, et al., Pharmaceutics 15 (2023) 1660.
[21] M. Hazeri, M. Faramarzi, S. Sadrizadeh, et al., J. Aerosol. Sci. 152 (2021) 105700.
[22] A. Grangier, J. Branchu, J. Volatron, et al., Adv. Drug Deliv. Rev. 176 (2021) 113843.
[23] R.G. Thorne, G.J. Pronk, V. Padmanabhan, W.H. Frey, Nat. Rev. 127 (2004) 481–496.
[24] T.P. Crowe, W.H. Hsu, Pharmaceutics 14 (2022) 629.
[25] G. Wang, Z. Zhai, W. Wang, et al., ACS Nano 18 (2024) 23684–23701.
[26] X. Yue, H. Guo, G. Wang, et al., Bioact. Mater. 44 (2025) 97–115.
[27] C. Hui, X. Li, Y. Liang, et al., Chin. Chem. Lett. 37 (2026) 111017.
[28] A.G. Shafik, H.A. Alkady, G.M. Tawfik, et al., Braz. J. Otorhinolaryngol. 86 (2020) 343–350.
[29] U.S. Food and Drug Administration, Bioavailability and bioequivalence studies for nasal aerosols and nasal sprays for local action, 2003. https://www.fda.gov/regulatory-information/search-fda-guidance-documents/bioavailability-and-bioequivalence-studies-nasal-aerosols-and-nasal-sprays-local-action.
[30] Z. Zhou, P. Hu, C. Qi, et al., Shock Vibrat. 2018 (2018) 8928120.